Geochemistry Geophysics Geosystems G3

Article
Volume 12, Number 6
24 June 2011
Q06012, doi:10.1029/2010GC003368
ISSN: 1525-2027

Published by AGU and the Geochemical Society

Thermometry of quartz mylonites: Importance of dynamic recrystallization on Ti-in-quartz reequilibration

Djordje Grujic
Department of Earth Sciences, Dalhousie University, Halifax, Nova Scotia B3H 4R2, Canada (dgrujic@dal.ca)

Michael Stipp
Department of Marine Geodynamics, Leibniz Institute of Marine Sciences at University of Kiel (IFM-GEOMAR), Wischhofstrasse 1-3, D-24148 Kiel, Germany

Joseph L. Wooden
Department of Geological and Environmental Science, Stanford University, Stanford, California 94305, USA

[1] Quartz mylonites from the Tonale Fault Zone in the Alps (northern Italy) have been investigated by the Ti-in-quartz geothermometer (TitaniQ) in order to test its applicability to measure deformation temperatures. The eastern part of the Tonale Fault Zone was contact metamorphosed by the synkinematic intrusion of the Adamello pluton, forming an ~800 m wide mylonitic shear zone, with a synkinematic temperature gradient from ~280°C at the frictional-viscous transition to ~700°C at the pluton contact as derived from metamorphic mineral assemblages. Deformation microstructures from quartz mylonite samples, systematically collected across the mylonitic shear zone, display the entire range of dynamic recrystallization in quartz, which comprise bulging recrystallization (BLG), subgrain rotation recrystallization (SGR), and grain boundary migration recrystallization (GBM). TitaniQ geothermometry yields the near-peak deformation temperature for quartz mylonites deformed at metamorphic temperatures above ~540°C in the zone of GBM. However, for mylonites formed under lower temperatures in the zones of SGR and BLG, the preexisting Ti concentrations were not reset. It is suggested that this is due to the sluggish Ti volume diffusion rates below 500°C and the short duration of contact metamorphism and deformation. Even in the higher temperature samples the reequilibration of Ti-in-quartz content was achieved by grain boundary migration rather than by volume diffusion. Hence, our results show that GBM is crucial for the reequilibration of Ti-in-quartz, while quartz mylonites deformed by either BLG or SGR, which predominate in natural shear zones at greenschist facies metamorphic conditions, most likely yield inherited temperatures.

Components: 13,800 words, 6 figures, 3 tables.

Keywords: Ti-in-quartz thermometry; dynamic recrystallization; mylonite; trace elements.

Index Terms: 1065 Geochemistry: Major and trace element geochemistry; 1115 Geochronology: Radioisotope geochronology; 5112 Physical Properties of Rocks: Microstructure.

Received 15 September 2010; **Revised** 7 April 2011; **Accepted** 14 April 2011; **Published** 24 June 2011.

Grujic, D., M. Stipp, and J. L. Wooden (2011), Thermometry of quartz mylonites: Importance of dynamic recrystallization on Ti-in-quartz reequilibration, *Geochem. Geophys. Geosyst.*, *12*, Q06012, doi:10.1029/2010GC003368.

1. Introduction

[2] Quartz mylonites are frequently found in shear zones of the continental crust, and development of their crystallographic preferred orientation (CPO = texture) and microstructure has been extensively studied in nature as well as through experimentation [e.g., *Tullis*, 2002]. To date, however, there is no reliable quantitative technique to directly determine their deformation temperature. The aluminum thermometer was proposed in 1970 [*Dennen et al.*, 1970], but it is not widely applied [e.g., *Götze et al.*, 2001]. The same is true for oxygen isotope thermometry [e.g., *Kirschner et al.*, 1995; *Mulch et al.*, 2007; *Vannay et al.*, 1999], which is rarely used owing to concerns about the influence of deformation and recrystallization, significantly different diffusion rates under different conditions, and the "potential existence of diffusional decoupling of oxygen isotope ratios" [*Cherniak and Watson*, 2007]. The recently developed Ti-in-quartz geothermometer (named TitaniQ by *Thomas et al.* [2010] and *Wark and Watson* [2006]) has been demonstrated to provide a reliable crystallization temperature of magmatic rocks [*Kawasaki and Osanai*, 2008; *Wark et al.*, 2007] as well as the metamorphic temperature of high and ultrahigh temperature metamorphic rocks [*Cherniak and Watson*, 2007; *Sato and Santhosh*, 2007]. The TitaniQ was developed under static experimental conditions, and for quartz neocrystallization. The question is how it could be applied for conditions of dynamic recrystallization in natural shear zones. It has been suggested that TitaniQ (calibration by *Wark and Watson* [2006]) can be applied to quartz mylonites [*Kohn and Northrup*, 2009; *Pennacchioni et al.*, 2010], but a systematic investigation of the geothermometer and its applicability with respect to the different dynamic recrystallization mechanisms of quartz is lacking. The TitaniQ has been experimentally calibrated for temperatures between 1000 and 600°C and extrapolated to temperatures as low as ~300°C [*Thomas et al.*, 2010; *Wark and Watson*, 2006], initially at 1 GPa only, but it has been recently demonstrated that a systematic decrease in Ti-in-quartz solubility occurs between 0.5 and 2 GPa [*Thomas et al.*, 2010]. Furthermore, because of the very low diffusion rates of Ti at relatively low temperatures [*Cherniak et al.*, 2007] and related sub-ppm Ti concentrations, TitaniQ application below 500°C is challenging, since there is a need for practical methods to measure precisely and accurately the low Ti-in-quartz concentrations. Thus, the outstanding questions related to Ti and other trace elements in quartz mylonites are as follows:

[3] a. Is the initial Ti-in-quartz concentration reset to new temperature conditions during crystal plastic (ductile) deformation?

[4] b. Can Ti-in-quartz concentrations successfully be measured down to deformation temperatures of 300°C?

[5] c. What is the effect of the different dynamic recrystallization mechanisms on Ti equilibration in quartz (and the distribution of the other trace elements)?

[6] In order to answer the above questions, TitaniQ was used to measure deformation temperatures of natural quartz mylonites deformed at a temperature range of ~280–700°C, displaying the full range of dynamic recrystallization microstructures of quartz characterized by bulging recrystallization (BLG), subgrain rotation recrystallization (SGR), and grain boundary migration recrystallization (GBM). The study area, in the Southern Alps (northern Italy), offers "laboratory conditions in nature" because of a well-constrained temperature, confining pressure, kinematics and timing of deformation [*Stipp et al.*, 2002a, 2002b, 2004].

2. Geological Setting and Sample Description

[7] Quartz mylonite samples were systematically collected across the eastern Tonale Fault Zone in the upper Val di Sole (Trentino, northern Italy, Figure 1). The Tonale Fault Zone is a dextral strike-slip segment of the largest Tertiary Fault Zone of the Alps, the Periadriatic Fault System [e.g., *Heitzmann*, 1987; *Schmid et al.*, 1989; *Stipp et al.*, 2004]. The eastern part of the Tonale Fault Zone was contact metamorphosed by the synkinematic Avio and Presanella intrusions of the Adamello pluton [*Stipp et al.*, 2004]. This segment of the Tonale Fault Zone consists of a paired mylonite belt, the Northern and the Southern Mylonite Zone (NMZ and SMZ), separated by the discrete Cataclastic Fault Zone (CFZ), while toward the west, the Tonale Fault Zone consists only of the NMZ and CFZ [*Stipp et al.*, 2004; *Werling*, 1992]. The SMZ of the eastern Tonale Fault Zone appears to have been formed only where the Fault Zone was in close vicinity to the Adamello pluton, suggesting a coupling between strike-slip shearing and contact metamorphism. The mylonitic foliation is vertical

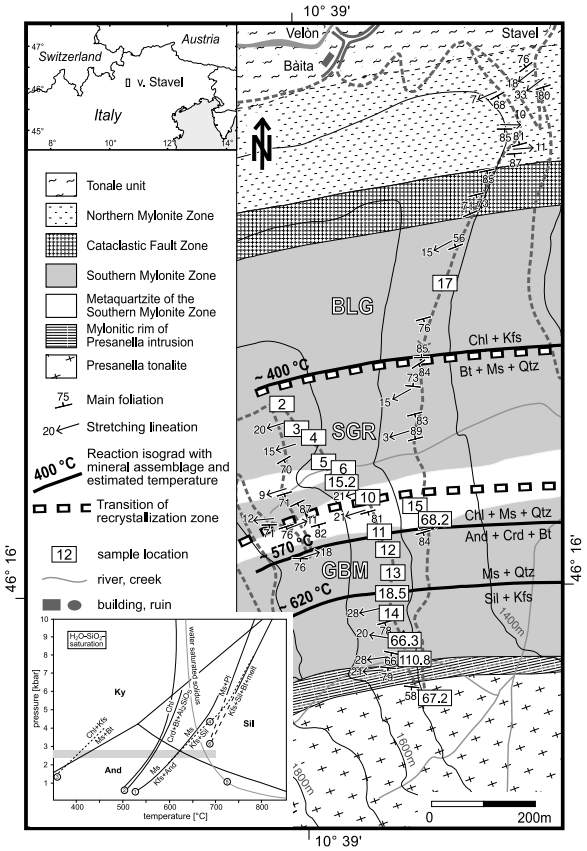

Figure 1. Map of the Val Stavel section with the locations of the analyzed samples, modified from *Stipp et al.* [2004]: BLG, zone of bulging recrystallization; SGR, zone of subgrain rotation recrystallization; GBM, zone of grain boundary migration recrystallization. Temperatures are inferred from the reaction isograds of critical mineral assemblages within the metasediments [*Stipp et al.*, 2002b]. Inset at the lower left shows the petrogenetic grid with synkinematic reactions observed along the section and the *P* and *T* ranges within the SMZ as estimated by *Stipp et al.* [2002b].

and strikes approximately ENE–WSW; the mylonitic stretching lineation plunges preferentially ~10° to the WSW (Figure 1). Dextral strike-slip shearing in the SMZ started at ~34.5 Ma [*Stipp et al.*, 2004]; i.e., simultaneously with or slightly after the emplacement of the Avio intrusion, and ceased by ~29 Ma when the Presanella intrusion of the Adamello pluton cooled below 300°C [*Del Moro et al.*, 1983; *Stipp et al.*, 2004]. The investigated rocks of the SMZ in the upper Val di Sole were penetratively deformed during Presanella contact metamorphism, reducing the time of interest to < ~2 Ma as will also be further constrained by new age dating of the Presanella tonalite presented in this study. Protoliths of the SMZ are the early Paleozoic Edolo schists [e.g., *Gansser and Pantic*, 1988], a monotonous series of phyllites with varying quartz content and intercalated quartzites. To the west, where they are not affected by Adamello contact metamorphism, the Edolo schists are characterized by pre-Alpine polyphase deformation under amphibolite and retrograde greenschist facies conditions [e.g., *Spalla et al.*, 1999].

[8] Across the ~800 m wide SMZ a synkinematic temperature gradient from ~280°C at the frictional-viscous transition (CFZ/SMZ transition) to ~700°C at the pluton contact was estimated using metamorphic reaction isograds [*Stipp et al.*, 2002b; *Werling*, 1992]. The confining pressure was constant at 250–300 MPa [*Stipp et al.*, 2002b] (Figure 1, inset). The inferred pressures and temperatures, thus, represent peak metamorphic conditions of deformation. Prior to pluton intrusion, the ambient temperature was estimated to be ~250°C [*Stipp et al.*, 2004]. The contact metamorphic temperature gradient displays a systematic change in peak temperature along the cross section, and thus from sample to sample. Corresponding deformation microstructures of mylonitic quartz veins display the entire range of dynamic recrystallization in quartz (Figure 2): BLG was dominant from ~280 to 400°C, SGR from ~400 to 510°C, and GBM from ~510 to 700°C [*Stipp et al.*, 2002b]. The peak metamorphic temperatures are, however, not necessarily the peak deformation temperatures registered in quartz because the ongoing deformation of the cooling contact aureole led to retrograde overprinting to variable extents of the peak temperature microstructures (Figure 2). Likewise, the concentration of Ti (and other trace elements in quartz) might have been locked in at some stage of this process rather than at the peak temperature conditions.

3. Methods

3.1. Sample Preparation

[9] Seventeen samples from the SMZ (Figure 1) were analyzed. Similar to the study by *Stipp et al.* [2002b], we also concentrated on the thin (<2 cm), deformed quartz veins oriented parallel to the mylonitic foliation. From these veins, 2–3 mm thin slices were cut perpendicular to the mylonitic foliation and parallel to the stretching lineation. The samples were broken, and fragments of ca. 2–3 mm across were mounted in 25 mm diameter epoxy disks with the cut surface (i.e., the kinematic plane) facing down. Sample surfaces were ground

and polished to provide a cross section through each sample. Before in situ trace element measurements, the samples were investigated using cathodoluminescence (CL) and backscattered electron imaging (BSE) in a scanning electron microscope to reveal any potential zoning in Ti concentration or any nonquartz impurities. The epoxy mounts were cleaned and coated with 70 nm Au before loading into the ion microprobe. In addition, standard thin sections of each sample were inspected with a petrographic microscope to identify the microstructures.

[10] Because of the coating and because the analyzed spots were selected with the aid of an optical camera inside the measurement chamber of the ion microprobe, there is little microstructural control on the spot locations. This is especially problematic in monomineralic rocks such as mylonitic quartz veins studied in this project. The analytical spots were selected away from inclusions, other mineral phases and pore spaces, and typical spacing between the spots was the estimated grain size. In samples with obvious bimodal grain size (e.g., TN11) the spacing was on the order of the recrystallized grain size to ensure that both porphyroclasts and recrystallized grains were measured.

3.2. Analytical Procedure

[11] All analyses were done on the SHRIMP-RG (Sensitive High Resolution Ion MicroProbe Reverse Geometry) in the U.S. Geological Survey-Stanford University ion microprobe facility in the School of Earth Sciences at Stanford University. A primary ion beam of 1 to 2.5 nA of negative O^{2-} was used to sputter secondary ions from the samples. A mass resolution of 6000 at 10% peak height eliminated any interference at the mass positions used for all elements except Sr. The run table included ^{7}Li, ^{9}Be, ^{11}B, ^{19}F, ^{23}Na, ^{26}Mg, ^{27}Al, ^{30}Si, ^{31}P, ^{32}S, ^{35}Cl, ^{39}K, ^{40}Ca, ^{47}Ti, ^{48}Ti, ^{49}Ti, ^{55}Mn, ^{56}Fe, ^{74}Ge, ^{85}Rb, ^{86}Sr, ^{88}Sr, and ^{93}Nb. Counting times of 2–4 s were used for elements other than Ti, with 4 s

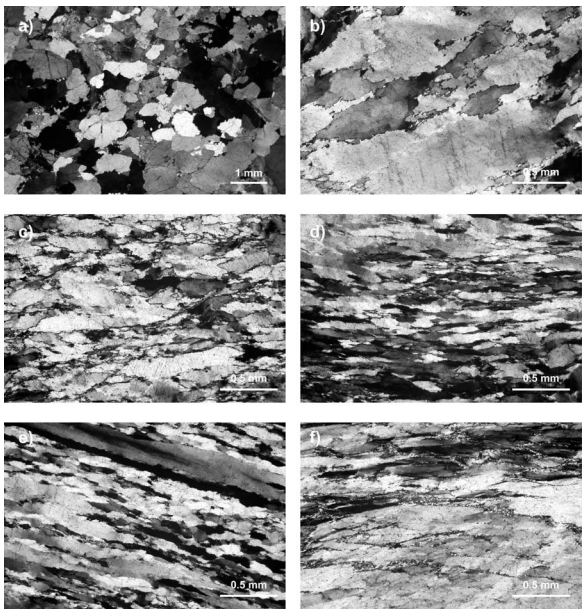

Figure 2. Micrographs of characteristic quartz microstructures of the investigated Tonale mylonites produced at different deformation temperatures. Peak synkinematic metamorphic temperature (T_{Met}) and TitaniQ temperature (T_{Ti}) are indicated. Crossed polarized light; scale bars are given for each image. See Figure 1 for specimen locations. (a) Sample from the migmatitic zone close to the intrusive contact: Quartz grains have large and irregular shapes and some lobate grain boundaries characteristic of the zone of GBM ($T_{Met} \approx 640°C$; $T_{Ti} \approx 645°C$; sample TN14). (b) Large, irregular and elongated porphyroclasts surrounded by smaller recrystallized grains. The recrystallized grains are about the same size as subgrains within the porphyroclasts. There are some small-scale sutures and bulges along the grain boundaries indicating a retrograde overprint by bulging recrystallization ($T_{Met} \approx 580°C$; $T_{Ti} \approx 555°C$; sample TN12). (c) Overprinting SGR microstructure from the GBM zone with large, irregular and elongated ribbon grains surrounded by smaller recrystallized grains. The porphyroclasts, with some relictic lobate grain boundaries, represent the original GBM microstructure of the sample ($T_{Ti} \approx 505°C$, porphyroclast cores). The recrystallized grains represent a retrograde overprint by SGR ($T_{Ti} \approx 435°C$, recrystallized mantle). Local bulging recrystallization with very small recrystallized grains overprints the entire microstructure ($T_{Met} \approx 565°C$; sample TN11). (d) Almost completely recrystallized microstructure with elongated recrystallized grains and a relictic porphyroclastic ribbon grain in the upper part of the image. This porphyroclast displays polygonization by subgrain formation, and the subgrains are about the size or slightly smaller than the recrystallized grains. This is the highest temperature sample of the zone of SGR and no reequilibration in Ti concentration could be determined. Some local overprint by bulging recrystallization is visible ($T_{Met} \approx 530°C$; $T_{Ti} \approx 363°C$; sample TN10). (e) Elongated ribbon grains surrounded by recrystallized grains characteristic of the zone of SGR. Recrystallized grains are about the same size or slightly larger than subgrains within the porphyroclastic ribbon grains ($T_{Met} \approx 500°C$; $T_{Ti} \approx 320°C$; sample TN6). (f) Large porphyroclasts with undulose and patchy extinction, internal shear bands, sutured grain boundaries, and recrystallized grains characteristic of the zone of BLG. Bulges, subgrains along the grain boundaries of the porphyroclasts and recrystallized grains are about the same size ($T_{Met} \approx 320°C$; $T_{Ti} \approx 320°C$; sample TN17).

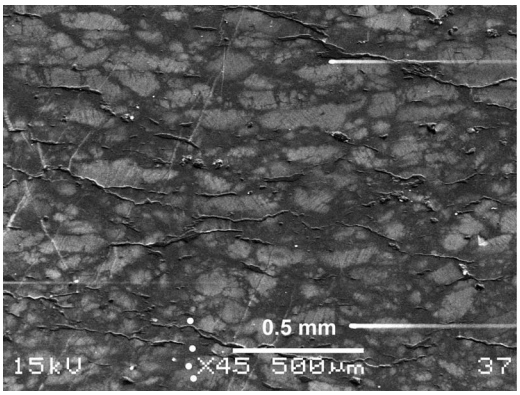

Figure 3. SEM cathodoluminescence (CL) image of sample TN11 with bright luminescent cores (porphyroclasts) in a darker matrix of recrystallized grains. Four measurement points are indicated (white dots), and acceleration voltage, magnification, scale bar and CL image number are given. Bright cores (TN11c) yield higher TitaniQ temperatures ($T_{Ti} \approx 505°C$), than those of the darker matrix (TN11r; $T_{Ti} \approx 433°C$).

for ^{48}Ti and 10 s for both ^{47}Ti and ^{49}Ti. Two or three scans through the run table were used for each analytical spot in each sample, with 10–25 spots being measured. The isotopic ratios between each of the 3 Ti isotopes were checked to ensure that there are no analytical interferences or counting problems. Background counts for all isotopes measured were insignificant. Data were reduced by determining average counts per second for each isotope and calculating a ratio with respect to ^{30}Si.

[12] Ti concentrations were calculated relative to a synthetic quartz doped to 46 ppm Ti (sample QTiP 13 by *Thomas et al.* [2010]). Quartz from a "lower temperature unit" of the Bishop tuff [*Wark et al.*, 2007]) was used as a secondary standard for Ti (average 40 ppm Ti). Concentrations of all other elements were relative to National Institute of Standards and Technology (NIST) Standard Reference Material (SRM) 610 and 612 and four rhyolite glasses – RLS-37, RLS-132, RLS-140, RLS-158 [*Macdonald et al.*, 1992] – using a correction for the difference in the silica concentrations between the NIST glasses and rhyolites (72–77 wt. % SiO_2) and the relative pure quartz. A calibration for Ti concentration was also determined using the NIST glasses and rhyolites and was within error to the more direct calibration determined from the synthetic quartz (QTiP 13). Ti concentrations in ppm were calculated from the equation given by *Wark et al.* [2007] and *Wark and Watson* [2006].

[13] The estimated 2σ accuracy of the TitaniQ thermometer in the temperature range between 700 and 400°C is ±4–5°C [*Wark and Watson*, 2006], while the analytical precision of the geothermometer using the SHRIMP-RG analyses was estimated to ±1–3°C in the same temperature range. Any error in the temperature estimate larger than ~10°C was therefore interpreted as within-sample variation between the analyzed spots/grains.

4. Results

4.1. Sample Description

[14] The majority of the samples are pure quartz veins within the schists, sample MS68.2 is a quartzite and three samples close to the magmatic contact (MS110.8, 66.3 and 18.5) are quartz-rich layers from migmatites. All the samples display a mylonitic foliation and stretching lineation parallel to those of the SMZ. Quartz veins occur in the whole SMZ and also in the Edolo schists unaffected by contact metamorphism and Tonale shearing. Most of the veins were therefore present in the original Edolo schists long before SMZ shearing; only a small number of veins were formed shortly before or during SMZ shearing as indicated by fiber grain porphyroclasts. The original Edolo schist veins outside the Adamello contact aureole preferentially consist of fairly isometric quartz grains with straight grain boundaries and coarse grain size (several hundred microns), indicative of annealing [*Stipp et al.*, 2004]. Original secondary microstructures with large irregular quartz grains and lobate grain boundaries are occasionally present as well. Textures are characterized by strong *c* axis maxima close to the periphery of the pole figure or incomplete girdle fabrics [*Stipp et al.*, 2002b, 2004]. These microfabrics suggest that the pre-Alpine retrograde greenschist facies deformation of the Edolo schist veins was insignificant, because low temperature BLG microstructures are completely lacking. Due to the long regional cooling time of the pre-Alpine metamorphism, the final Ti content has possibly been controlled by volume diffusion. The SMZ quartz veins display uniform, featureless CL with the exception of sample TN11, in which the elliptical bright cores (the porphyroclasts) are surrounded by darker gray rims (recrystallized matrix) (Figure 3).

[15] Samples TN11-TN15, 110.8, 66.3, 68.2 and 18.5 are from the GBM zone (Figure 1) [cf. *Stipp*

et al., 2002b]. Their microstructures are characterized by large irregular grains, lobate grain boundaries, and dissection microstructures (Figures 2a and 2b) [*Jessell*, 1987; *Stipp et al.*, 2002b; *Urai et al.*, 1986]. These GBM grains were overprinted to a different extent by retrograde SGR and some local BLG (Figures 2b and 2c). Large GBM grains (>200 μm) dominate the microstructure within all the GBM zone samples, except for sample TN11 in which the retrograde overprint is strong, with a high percentage of dynamic recrystallization (Figure 2c). Nevertheless, there are porphyroclasts left in TN11 which show no transformation into elongated ribbon grains but rather irregular grain shapes and lobate grain boundaries, suggesting a previous GBM activity.

[16] There is a broad transitional zone between GBM and SGR without samples within the study by *Stipp et al.* [2002b]. We did find a sample (TN10) in this zone with an inhomogeneous microstructure and considerable retrograde overprinting by BLG. The highest temperature/lowest stress microstructure, however, consists of relic elongated porphyroclasts embedded in a matrix of recrystallized grains (Figure 2d). These recrystallized grains are also elongated and about the size or slightly larger than the subgrains inside the porphyroclasts (Figure 2d). The partly sutured-to-lobate grain boundaries of the recrystallized grains may indicate a contribution of grain boundary migration close to the SGR/GBM transition, as already proposed for sample MS15.2 [cf. *Stipp et al.*, 2002b, Figure 3f]. The recrystallized grain size of sample TN10 is approximately 100–110 μm when taking the strong shape fabric into account [cf. *Stipp et al.*, 2002a, 2002b]. Hence, this size is close to 120 μm, which has been reported to be the characteristic recrystallized grain size at the SGR/GBM transition based on a worldwide compilation of quartz mylonite samples [*Stipp et al.*, 2010]. Sample TN10 allows us therefore to locate more precisely and accurately the SGR/GBM transition in the investigated transect across the Tonale Fault Zone; i.e., between samples TN10 and TN15 at a peak synkinematic temperature of ~540°C (Figure 1).

[17] Samples TN2–TN6, and 15.2 [cf. *Stipp et al.*, 2002a] show typical SGR microstructures with elongated ribbon grains (porphyroclasts) surrounded by recrystallized grains that are about the same size or slightly larger than the subgrains within the porphyroclasts (Figure 2e). The porphyroclasts are interpreted as being remnants of the pre-SMZ grains; i.e., they were presumably formed during pre-Alpine metamorphism and deformation (cf. above in the same section). Retrograde overprints in the SGR zone [cf. *Stipp et al.*, 2002b] are characterized by sutured or serrated grain boundaries, indicative of BLG, whereas the grain boundary bulges, mantle subgrains [e.g., *Valcke*, 2008], and small recrystallized grains are about the same size. This overprinting can be quite intense in the samples.

[18] The BLG/SGR transitions at a recrystallized grain size of 35–40 μm [*Stipp et al.*, 2010] is not well represented in our sample set. TN17, the only sample collected from the BLG zone, contains large porphyroclasts with undulose and patchy extinction, internal shear band sets, and sutured grain boundaries (Figure 2f). Bulges along the grain boundaries, mantle subgrains, and recrystallized grains are approximately the same size.

4.2. Trace Element Concentrations

[19] In addition to Ti, five trace elements were examined (Li, Al, P, Fe, Ge), for which the concentration was adequately high to warrant analytical precision, and for which the position in the crystal lattice of quartz is known [e.g., *Götze et al.*, 2001; *Larsen et al.*, 2004; *Maschmeyer and Lehmann*, 1983; *Rakov*, 2006]. The concentration of these trace elements was normalized to ^{30}Si. The relative concentrations of ^{7}Li, ^{27}Al, ^{48}Ti and ^{56}Fe decrease with distance from the pluton, with a break in slope at approximately 300 m from the contact for the first three and at about 150 m for Fe (Figure 4). Beyond this distance the concentrations appear to be constant within the error. There is no clear trend for *P* and ^{74}Ge concentrations. These data suggest that the change in concentration of different trace elements (especially Ti, Al and perhaps Fe) is not only a function of recrystallization temperature but also of respective diffusivity rates. Li^{+}, being a very mobile and an interstitial trace element that acts as a charge compensator with Al^{3+} and Fe^{3+}, likely changes its concentration as a function of the other two trace elements, replacing Si^{4+}. If the change of studied trace element concentration was simply the result of metamorphic fluids emanating from the pluton, the break in concentration/distance slope would be at approximately the same distance from the pluton as where the fluid infiltration ceased.

4.3. Titanium-in-Quartz Geothermometry (TitaniQ)

[20] Temperature was calculated for each analytical spot and, for each sample, the average value is

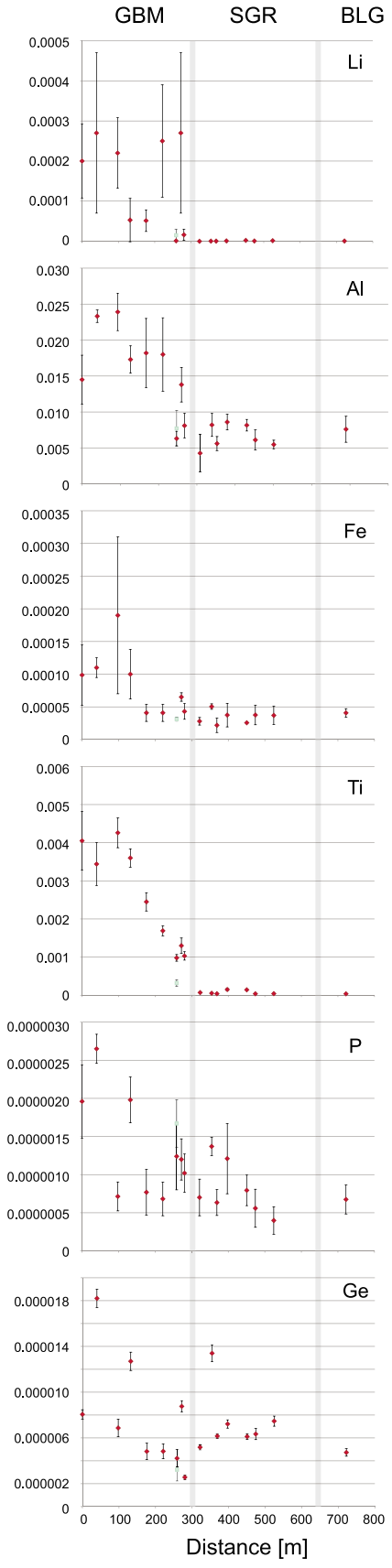

reported (Table 1). TitaniQ temperatures were determined using equation 12 of *Thomas et al.* [2010]:

$$T(^{\circ}C) = \frac{a + c \times P}{b - R \times \ln X_{TiO_2}^{Qtz} + R \times \ln a_{TiO_2}} - 273.15 \quad (1)$$

The parameters a, b and c were the same as given by *Thomas et al.* [2010]. R is the gas constant 8.314472 J K^{-1} mol^{-1}. The $X_{TiO_2}^{Qtz}$ is the mole fraction of TiO_2-in-quartz converted from the measured Ti concentration (in ppm) using *Thomas et al.*'s [2010, appendix] equation.

[21] As the SMZ is a dominantly strike-slip shear zone, there was no significant differential uplift across the shear zone; therefore the confining pressure was assumed to be 275 ± 25 MPa for all the studied samples. Ti activity (a_{TiO2}) in monomineralic rocks, as in quartz veins, is difficult to estimate. Although rutile, ilmenite and magnetite were observed in several of the samples, no reactions between FeTi oxides could be found, which would be required as exchange reactions to calculate the a_{TiO2}. Dynamic recrystallization of quartz was driven by deformation and differential stress, not by metamorphic reactions. Coexisting FeTi oxides, formed likely during precipitation of the studied veins, did not recrystallize together with quartz during shearing. In addition, some rutile needles may have formed by exsolution of Ti from the quartz lattice during cooling [e.g., *Cherniak and Watson*, 2007]. Therefore, even where FeTi oxides are present, assuming ideal exchange equilibria between them would not apply for the a_{TiO2} during dynamic recrystallization of quartz. The minimum synkinematic a_{TiO2} was thus calculated

Figure 4. Trace element concentrations with respect to distance from the intrusion. Concentrations of the trace elements are shown as a ratio to ^{30}Si. Sample TN11 is subdivided into porphyroclasts (TN11c; red symbol) and recrystallized grains (TN11r; green symbol). The porphyroclasts formed by GBM are close to peak synkinematic temperature within the GBM zone, and the recrystallized grains by SGR under retrograde conditions. Vertical gray stripes mark the transitions between dominant dynamic recrystallization mechanisms: GBM, grain boundary migration recrystallization; SGR, subgrain rotation recrystallization; BLG, bulging recrystallization. The horizontal error bar is 2σ = ±5 m and smaller than the symbol, the vertical error bar represents the standard deviation of the measurements within the sample. Note that for Li, Al, Ti and Fe the standard deviation is larger in the zone of GBM than in the zones of SGR and BLG where no changes in concentration with distance (i.e., temperature) occur.

Table 1 (Sample). Ti Content and Calculated TitaniQ Temperatures[a] [The full Table 1 is available in the HTML version of this article]

Sample-Spot Number	^{49}Ti (ppm)	^{49}Ti (mol)	T (°C) (2006)	T at 2.75 kbar, a_{TiO2} = 1	T at 2.75 kbar, a_{TiO2} = 0.5	T at 2.75 kbar, a_{TiO2} = 0.3	T at 2.75 kbar, a_{TiO2} = 0.2
TN02-01	0.3249	4.08E-07	336.39	257.67	283.58	304.35	321.97
TN02-02	0.2804	3.52E-07	330.15	252.48	277.87	298.21	315.45
TN02-03	0.3240	4.07E-07	336.28	257.58	283.48	304.24	321.86
TN02-04	0.3817	4.79E-07	343.37	263.48	289.97	311.23	329.28
TN02-05	0.3271	4.11E-07	336.69	257.92	283.85	304.64	322.28
TN02-06	0.4053	5.09E-07	346.02	265.68	292.39	313.84	332.06
TN02-07	0.3256	4.09E-07	336.49	257.75	283.67	304.44	322.07
TN02-08	0.2902	3.64E-07	331.60	253.69	279.20	299.64	316.97
TN02-09	0.3193	4.01E-07	335.65	257.06	282.90	303.62	321.20
TN02-10	0.3334	4.19E-07	337.50	258.60	284.60	305.45	323.14
TN02			**337.00 ± 4.73**	**257.80 ± 0.40**	283.67 ± 0.48	304.45 ± 0.52	322.08 ± 0.55
TN03-01	0.3275	4.11E-07	336.74	257.96	283.90	304.69	322.34
TN03-02	0.3340	4.19E-07	337.58	258.66	284.66	305.52	323.21
TN03-03	0.3339	4.19E-07	337.56	258.65	284.65	305.51	323.20
TN03-04	0.3166	3.97E-07	335.29	256.76	282.57	303.27	320.83
TN03-05	0.2408	3.02E-07	323.83	247.21	272.08	291.99	308.86
TN03-06	0.3291	4.13E-07	336.95	258.14	284.09	304.90	322.56
TN03-07	0.3787	4.75E-07	343.04	263.20	289.66	310.90	328.93
TN03-08	0.3614	4.54E-07	340.99	261.50	287.79	308.88	326.79
TN03-09	0.3668	4.60E-07	341.64	262.03	288.38	309.52	327.46
TN03-10	0.3412	4.28E-07	338.51	259.43	285.51	306.43	324.19
TN03			**337.00 ± 5.30**	**259.30 ± 1.90**	285.40 ± 2.10	306.30 ± 2.30	324.00 ± 2.40
TN04-01	1.1483	1.44E-06	395.74	306.83	337.90	363.02	384.47
TN04-02	1.1803	1.48E-06	397.17	308.01	339.20	364.43	385.98
TN04-03	1.6627	2.09E-06	415.40	323.02	355.90	382.55	405.36
TN04-04	1.2162	1.53E-06	398.72	309.29	340.63	365.97	387.63
TN04-05	1.1595	1.46E-06	396.25	307.25	338.36	363.52	385.01
TN04-06	1.1929	1.50E-06	397.72	308.46	339.71	364.98	386.57
TN04-07	1.1170	1.40E-06	394.32	305.66	336.60	361.61	382.96
TN04-08	1.0877	1.37E-06	392.96	304.54	335.35	360.26	381.52
TN04-09	1.1210	1.41E-06	394.51	305.81	336.77	361.79	383.16
TN04-10	0.9950	1.25E-06	388.43	300.80	331.21	355.77	376.73
TN04			**397.00 ± 7.05**	**306.40 ± 1.80**	337.50 ± 2.00	362.50 ± 2.20	384.00 ± 2.30
TN05-01	0.7782	9.77E-07	376.26	290.74	320.07	343.71	363.86
TN05-02	0.7301	9.16E-07	373.17	288.19	317.24	340.65	360.60
TN05-03	0.6624	8.31E-07	368.52	284.33	312.98	336.05	355.69
TN05-04	1.2835	1.61E-06	401.54	311.61	343.20	368.77	390.62
TN05-05	1.0284	1.29E-06	390.10	302.18	332.74	357.42	378.49
TN05-06	1.4364	1.80E-06	407.50	316.52	348.66	374.69	396.95
TN05-07	1.3377	1.68E-06	403.72	313.41	345.20	370.93	392.93
TN05-08	1.1832	1.49E-06	397.29	308.11	339.32	364.55	386.11
TN05-09	1.1047	1.39E-06	393.76	305.19	336.08	361.04	382.36
TN05-10	1.5778	1.98E-06	412.55	320.67	353.29	379.71	402.32
TN05			**392.00 ± 15.19**	**304.30 ± 9.40**	335.00 ± 10.00	360.00 ± 11.00	381.00 ± 12.00
TN06-01	0.4397	5.52E-07	349.64	268.69	295.71	317.41	335.85
TN06-02	0.2846	3.57E-07	330.78	253.00	278.44	298.83	316.11
TN06-03	0.3275	4.11E-07	336.74	257.96	283.90	304.69	322.34
TN06-04	0.3444	4.32E-07	338.90	259.76	285.87	306.82	324.60
TN06-05	0.2465	3.09E-07	324.80	248.02	272.97	292.94	309.87
TN06-06	0.2645	3.32E-07	327.71	250.45	275.64	295.81	312.91
TN06-07	0.2814	3.53E-07	330.30	252.61	278.01	298.36	315.61
TN06-08	0.3662	4.60E-07	341.56	261.97	288.31	309.44	327.38
TN06-09	0.3035	3.81E-07	333.49	255.25	280.92	301.49	318.94
TN06-10	0.2077	2.61E-07	317.81	242.19	266.57	286.07	302.58

[a]Measured concentration of Ti and mol fraction are calculated after *Thomas et al.* [2010]. Using TitaniQ, the temperature is calculated for each analytical spot, and for each sample the average values are reported. The average Tukey's Biweight analysis was performed [*Press et al.*, 1992], in which the outlier values are ignored. Temperatures are calculated according to *Wark and Watson* [2006] (a_{TiO2} = 1.0), *Thomas et al.* [2010] (*P* 275 MPa, a_{TiO2} = 0.5), *Thomas et al.* [2010] (275 MPa, a_{TiO2} = 0.3), and *Thomas et al.* [2010] (*P* 275 MPa, a_{TiO2} = 0.2). For sample TN11, values for cores (TN11c) and recrystallized mantles (TN11r) are listed. Ti-in-quartz concentrations for the reference sample QTiP 13 [*Thomas et al.*, 2010] are also given. Italic values are data outliers, which are not used for the calibration. Mean values in bold are described in the text, and mean values in plain text are for comparison purposes only.

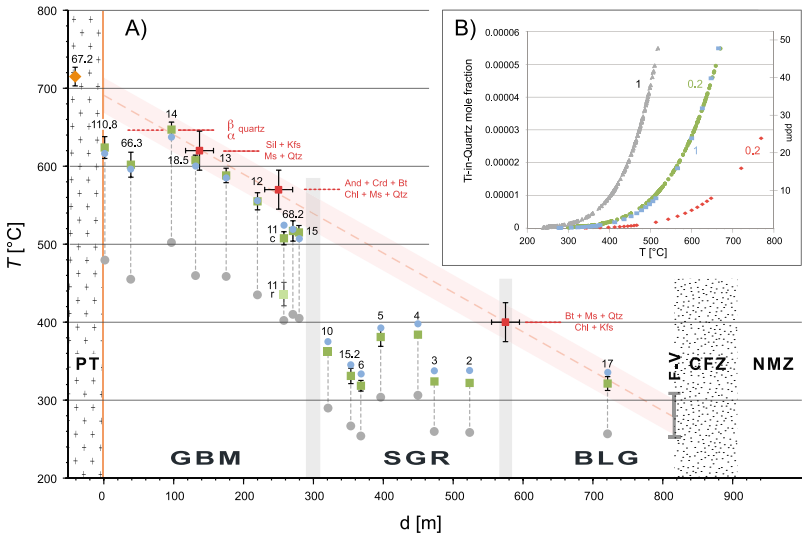

Figure 5. (a) Temperatures calculated with the TitaniQ as a function of distance of the samples from the intrusive contact. The locations and temperature ranges of the metamorphic isograds are marked in red and labeled as in Figure 1. The quartz $\alpha-\beta$ transition at 250–300 MPa after *Shen et al.* [1993] is also indicated. The orange symbol illustrates the crystallization temperature of the Presanella tonalite estimated by Ti in zircon geothermometry (see section 4.4). Vertical gray stripes indicate the transitions in the dynamic recrystallization mechanisms of quartz [*Stipp et al.*, 2002b]. GBM: zone of dominant grain boundary migration recrystallization; SGR: zone of dominant subgrain rotation recrystallization; BLG: zone of dominant bulging recrystallization; CFZ: cataclastic fault zone; NMZ: northern mylonite zone; PT: Presanella tonalite; F-V: frictional-viscous transition. TitaniQ temperatures after *Thomas et al.* [2010] are shown for P = 275 MPa and a_{TiO2} = 0.2 (green symbols), and for P = 275 MPa and a_{TiO2} = 1.0 (gray circles connected with dashed lines to the corresponding green symbols). Note the difference in temperature in sample TN11 between hot porphyroclast cores (*c*) and colder recrystallized mantles (*r*). TitaniQ temperatures after *Wark and Watson* [2006] (aTiO2 = 1.0) are shown by blue circles. Errors represent only within sample variations and do not account for uncertainties of TitaniQ calibration, a_{TiO2} and P. Error bars for samples TN2–4 and TN10 are smaller than the symbols; error bars for gray and blue symbols are omitted for clarity. (b) Ti in quartz mole fractions (left ordinate) versus temperatures are calculated after *Thomas et al.* [2010]. All analytical spots are indicated. Temperatures are calculated for P = 275 MPa and aTiO2 = 0.2 (green symbols) and aTiO2 = 1 (gray symbols). Concentrations in ppm (right ordinate) versus calculated temperatures for the *Wark and Watson* [2006] calibration for 25 points with equal spacing in Ti-in-quartz mole fractions; aTiO2 = 0.2 (red symbols), aTiO2 = 1 (blue symbols). Note that with increasing Ti-in-quartz concentrations the difference in temperature increases for different aTiO2 values.

using the sample TN14 with the highest Ti-in-quartz concentration, the local peak synkinematic temperature of 630°C ± 30°C (see Figures 1 and 3) as the maximum temperature permitted during dynamic quartz recrystallization, and by rearranging equation (1) to:

$$\ln a_{TiO_2} = \frac{a + c \times P}{R \times (T + 273.15)} - \frac{b}{R} + \ln X_{TiO_2}^{Qtz} \qquad (2)$$

The average a_{TiO2} = 0.20 ± 0.02 was obtained for 10 analytical spots in the sample, and a_{TiO2} = 0.2 was then applied to all calculations, with obtained results then interpreted as maximum deformational temperatures. The greatest possible a_{TiO2} for the GBM samples was estimated to be ~0.3, because at higher values the calculated deformation temperature would be lower than the temperature required to produce the observed deformational microstructures (see further discussion in section 5.2).

[22] The Ti-in-quartz concentration of the entire sample set varies between 0.2 and 44 ppm (2.56E-7 to 5.48E-5 mol fractions), yielding individual spot temperatures between ~302 and ~670°C. The average temperatures of the samples range from 319 to 647°C. Within the first 300 m, from the contact to the pluton, a continuous decrease in temperature, from ~650 to ~515°C, is observed within the zone of GBM (Figure 5). Within analytical error, this trend is consistent with the peak temperatures from synkinematic reaction isograds [*Stipp et al.*, 2002b; *Werling*, 1992], which display an almost linear decrease in temperature across the SMZ (Figure 5). In sample TN11, there is a clear bimodal distribution of the calculated temperatures; the brighter CL cores and the darker CL rims yielded 505°C and 433°C respectively (Figure 5). The GBM-SGR transition between the samples TN15 and TN10 is rather distinct, with a decrease in

Table 2. Shrimp U-Pb Isotopic Analyses for Zircon[a]

Spot	U (ppm)	Th (ppm)	Th/U	$^{204}Pb/^{206}Pb$	Common ^{206}Pb (%)	$^{238}U/^{206}Pb$[b]	Error (%)	$^{207}Pb/^{206}Pb$[b]	Error (%)	$^{206}Pb/^{238}U$ Age[c] (Ma)	Error (%)
MS2-1	*152*	*39*	*0.26*	*5.2E-3*	*2.39*	*193.87*	*1.5*	*0.0655*	*7.0*	*32.4*	*0.5*
MS2-3	204	68	0.34	2.4E-3	0.30	208.14	1.4	0.0490	6.2	30.8	0.5
MS2-4	224	75	0.34	1.2E-3	0.34	210.31	1.2	0.0493	5.4	30.5	0.4
MS2-5	158	38	0.25	1.9E-3	1.77	209.67	1.5	0.0606	6.0	30.1	0.5
MS2-7	303	79	0.27	-	0.11	210.01	1.1	0.0475	6.8	30.6	0.4
MS2-7	841	105	0.13	1.6E-2	29.57	147.16	0.6	0.2805	2.0	30.8	0.4
MS2-8	*512*	*119*	*0.24*	-	*0.93*	*77.51*	*0.7*	*0.0551*	*2.6*	*81.9*	*0.6*
MS2-9	187	63	0.35	2.0E-2	24.26	163.93	1.4	0.2385	6.2	29.7	0.8
MS2-10	160	45	0.29	1.8E-3	0.85	210.06	1.6	0.0533	6.8	30.4	0.5
MS2-11	158	54	0.36	2.0E-3	1.55	201.30	1.6	0.0589	6.8	31.5	0.5
MS2-12	121	42	0.36	2.6E-3	7.70	202.32	1.6	0.1075	15.3	29.3	0.8
MS2-13	*241*	*79*	*0.34*	-	*0.39*	*192.44*	*1.3*	*0.0498*	*5.6*	*33.3*	*0.5*
MS2-14	*272*	*94*	*0.36*	*1.4E-3*	*−0.28*	*200.38*	*1.2*	*0.0444*	*5.3*	*32.2*	*0.4*
MS2-15	390	219	0.58	-	0.72	204.87	1.0	0.0523	4.1	31.2	0.3
MS2-16	251	76	0.31	2.6E-3	2.14	203.52	1.3	0.0636	4.8	30.9	0.4

[a]Errors quoted in Table 2 are listed at 1σ, but where data are combined for regression analysis or weighted mean age, the final result is quoted within the 95% confidence limits. Italic values are outliers, and the corresponding measurements were not used for age calculations.
[b]Uncorrected values.
[c]Corrected for ^{207}Pb.

TitaniQ temperature from 515 to 363°C respectively. Further north, within the zones of SGR and BLG, the TitaniQ temperatures scatter between ~320 and ~385°C without any consistent trend of decreasing temperature and without correlation to the recrystallization mechanism transition (Figure 5). Temperatures based on $a_{TiO2} = 1$ and on the calibration of *Wark and Watson* [2006] with $a_{TiO2} = 1$ are shown for comparison. Two pairs of curves of T calculated for $a_{TiO2} = 0.2$ and 1 are shown in Figure 5b, one after *Wark and Watson* [2006], the other after *Thomas et al.* [2010] to illustrate the increase in temperature difference with increasing Ti content.

4.4. Timing of Contact Metamorphism

[23] New geochronological and geothermometer measurements were carried out to better constrain intrusion ages and temperatures at the rim of the Adamello pluton [cf. *Stipp et al.*, 2004]. Zircons from a tonalite sample (MS97–67.2, Figure 1) were analyzed for U-Pb and trace element composition using the SHRIMP-RG. Mineral separates were the same as those used by *Stipp et al.* [2004]. Fifteen spots from 11 zircon grains were analyzed. Pits were ~30 μm in diameter and had a depth of ~5 μm. Analytical procedures are outlined in the auxiliary material, with results presented in Table 2 and plotted in Figure 6.[1] A group of eleven concordant spots are combined to a weighted $^{206}Pb/^{238}U$ mean age of 30.5 ± 0.5 Ma (mean square weighted deviation, MSWD = 0.48). This date is confirmed by a TuffZirc Age of 30.59 +0.33/−0.46 Ma (Figure 6b) calculated using Isoplot/Ex 3.0 as defined by *Ludwig and Mundil* [2002].

[24] The crystallization temperature of zircon was estimated using Ti-in-zircon geothermometry [*Watson et al.*, 2006]. Spot locations were the same as for U-Pb analyses of the same zircons: analytical procedures are provided in the auxiliary material. Data collected from zircon rims and the temperatures calculated using the calibration of *Ferry and Watson* [2007] are shown in Table 3. The temperatures range from 703.5 to 741.6°C for individual spots, yielding an average temperature of 715 ± 12°C. This temperature, at the rim of the Presanella tonalite, fits very well to the observed partial melting of the closest metapelitic to metapsammitic rocks during contact metamorphism at ~650–700°C or higher [*Stipp et al.*, 2002b, 2004] and thus to the apparent temperature gradient in the contact aureole (Figure 5) [*Stipp et al.*, 2002b].

5. Discussion

5.1. Contact Metamorphism and Shearing

[25] It has been suggested that the whole thermal pulse within the SMZ did not last longer than ~5 Ma and was probably much shorter than that [*Stipp et al.*, 2004]. The observed apparent thermal

[1]Auxiliary materials are available in the HTML. doi:10.1029/2010GC003368.

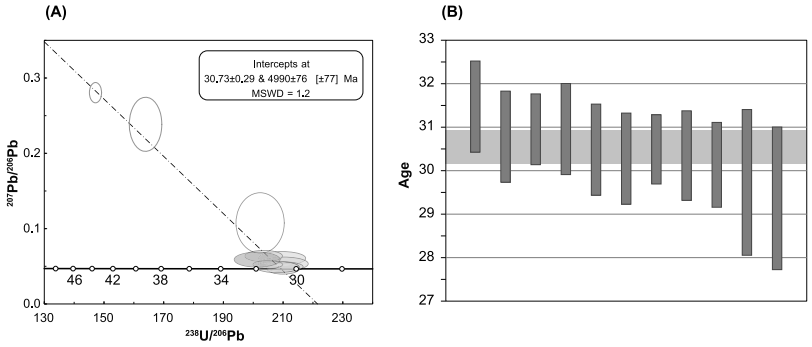

Figure 6. SHRIMP U-Pb geochronology of zircon grains from the Presanella tonalite: (a) Tera-Wasserburg concordia diagram: intercepts are at 30.73 ± 0.29 and 4990 ± 76, MSWD = 1.2. Data point error ellipses are 2σ. (b) TuffZirc Age of 30.59 + 0.33–0.46 Ma with a 93.5% confidence from a coherent group of 11 ages: box heights are 2σ. All the geochronological statistical assessments were performed using the Isoplot/Ex 3.0 program of *Ludwig* [2003].

gradient in the contact aureole was caused by the strike-slip motion across the Tonale Fault Zone, which continuously brought cooler rocks (ambient temperature of ~250°C) against the evolving aureole. Hence, advective cooling severely perturbed the temperature trend across the northern Adamello contact aureole [*Stipp et al.*, 2004].

[26] The new age of tonalite crystallization of 30.5 ± 0.5 Ma, the youngest date yet, confirms that the Presanella tonalite is the youngest intrusion in the complex Adamello batholith [cf. *Del Moro et al.*, 1983; *Hansmann and Oberli*, 1991; *Mayer et al.*, 2003; *Pomella et al.*, 2011; *Stipp et al.*, 2004]. The average Ti-in-zircon temperature of 715.0 ± 12.0°C is interpreted as *T* of Presanella tonalite crystallization at 30–31 Ma. In combination with the Rb/Sr cooling age of muscovite (31 Ma) and the K/Ar and Rb/Sr cooling ages of biotite (32–29 Ma), both by *Del Moro et al.* [1983], this indicates fast cooling below 300°C to the preintrusion ambient temperature immediately after the intrusion, even faster cooling than that based on the hitherto available U/Pb zircon age of 32.0 ± 2.3 Ma [*Pennacchioni et al.*, 2006; *Stipp et al.*, 2004]. Time of mylonitization at peak temperature conditions at any site of the contact aureole was, accordingly, very short, probably from a few 10 ka close to the pluton to not more than 1 Ma in the outermost parts of the SMZ [*Stipp et al.*, 2004].

5.2. Titanium Activity

[27] It has been suggested that metapelitic rocks, which usually contain abundant FeTi oxides, have the a_{TiO2} of 1 or close to 1 [*Ghent and Stout*, 1984].

Table 3. Ti-in-Zircon Data[a]

Spot	^{48}Ti (ppm)	^{49}Ti (ppm)	T (°C), a_{TiO2} = 0.7	Error[b] (2σ)	Age (Ma)	Error (2σ)	Fe (ppm)	Hf (ppm)
MS97672-2.1	4.6	4.6	708.0	20	*32.4*	*0.5*	1	11558
MS97672-2.2	*1.8*	*1.9*	*635.1*	*20*	–	–	*81*	*18298*
MS97672-2.3	4.9	5.4	722.9	20	30.8	0.5	1	10729
MS97672-2.4	4.9	4.9	713.0	20	30.5	0.4	0	9999
MS97672-2.5	5.3	4.8	711.8	20	30.1	0.5	2	11798
MS97672-2.6	*2.9*	*2.9*	*668.9*	*20*	–	–	*1675*	*14303*
MS97672-2.7	2.2	1.9	636.9	20	30.8	0.4	1	11722
MS97672-2.8	3.9	3.8	692.7	20	*81.9*	*0.6*	1	11994
MS97672-2.9	4.8	5.4	722.4	20	29.7	0.8	1	10621
MS97672-2.10	4.3	4.3	701.5	20	30.4	0.5	0	11028
MS97672-2.11	4.9	4.8	711.2	20	31.5	0.5	1	10433
MS97672-2.12	4.6	4.6	707.0	20	29.3	0.8	1	10646
MS97672-2.13	3.1	3.1	674.2	20	*33.3*	*0.5*	1	12802
MS97672-2.14	5.3	5.5	723.4	20	*32.2*	*0.4*	1	9617
MS97672-2.15	6.5	6.7	741.6	20	31.2	0.3	1	10695
MS97672-2.16	4.2	4.4	703.5	20	30.9	0.4	1	11701

[a]Temperatures were calculated using calibrations from *Ferry and Watson* [2007]. Italic values were not used for the average temperature calculation because of anomalously high Fe content.
[b]Estimated from error in empirical correlation [*Ferry and Watson*, 2007].

Since rutile and also some ilmenite and magnetite were found in the metapelitic to metapsammitic series and also in some of the quartz vein samples, $a_{TiO2} = 1$ was initially assumed for the temperature calculations with the TitaniQ calibration by *Wark and Watson* [2006] as has been done by the first studies on quartz mylonites [*Grujic et al.*, 2009; *Kohn and Northrup*, 2009; *Pennacchioni et al.*, 2010]. This provided results, interpreted as minimum temperatures, which are consistent with the estimations of the peak synkinematic temperature within error of ±30°C [cf. *Stipp et al.*, 2002b]. It should be noted that for $a_{TiO2} < 0.7$ the deformation temperatures of the hottest samples TN12–14 would be higher than the peak synkinematic temperatures, including the 30°C error of the metamorphic reactions and the 12°C standard deviation of measurements in these samples. However, it was found experimentally that the Ti solubility in quartz is highly pressure dependent [*Thomas et al.*, 2010]. Consequently, we used the pressure-dependent TitaniQ calibration of *Thomas et al.* [2010] with $a_{TiO2} = 1$ and $P = 275$ MPa that conversely yields up to 150°C lower temperatures than the corresponding peak synkinematic metamorphic temperatures and also significantly lower than the temperatures required to form the observed dynamic recrystallization microstructures (Table 1 and Figure 5). For example, in several samples with BLG and SGR microstructures, a deformation temperature well below the frictional-viscous or brittle-plastic transition (BPT) at 270–310°C [e.g., *Stipp et al.*, 2002b; *Stöckhert et al.*, 1999; *van Daalen et al.*, 1999; *Voll*, 1976] was indicated. At such low temperatures dominant plastic deformation of quartz is impossible because of a required differential stress above the confining pressure, which automatically causes a switch from plastic to brittle deformation (Goetze criterion) [e.g., *Kohlstedt et al.*, 1995]. Therefore, the temperature estimation must either be wrong or does not correspond to the mylonitization of the rock but to a deformation at retrograde conditions. The latter can be excluded due to the sluggish Ti diffusion in quartz at temperatures below 300°C (see also section 5.4).

[28] As described in section 4.3, the minimum a_{TiO2} for the sample with the highest Ti-in-quartz content was estimated, assuming that the local peak synkinematic temperature is the highest temperature achieved during dynamic recrystallization of quartz. The $a_{TiO2} = 0.2$ yielded temperatures closest to the local peak synkinematic temperatures (Table 1 and Figure 5a). Lower a_{TiO2} is not possible because the TitaniQ temperature in the hottest samples would be higher than the metamorphic temperature or even the intrusion. Conversely, maximum a_{TiO2} for the GBM samples is ~0.3, because at higher values the calculated deformation temperature would be lower than the temperature required for dynamic recrystallization and plastic flow (e.g., conflict with Goetze criterion as discussed above). Likewise, inserting an $a_{TiO2} = 0.2$ into the TitaniQ equation of *Wark and Watson* [2006] yields geologically unrealistically high temperatures (Figure 5b) which is caused by an overestimation of pressure since, in that study, the Ti solubility in quartz was determined along only one isobar (1 GPa). To test these parameters, temperatures given by *Kohn and Northrup* [2009] (based on the *Wark and Watson* [2006] calibration and $a_{TiO2} = 1$) were recalculated using a confining pressure of 400 ± 100 MPa [*Kohn and Northrup*, 2009; M. Kohn, personal communication, 2009], published Ti-in-quartz concentrations [*Kohn and Northrup*, 2009] and the pressure-dependent Ti-in-quartz calibrations by *Thomas et al.* [2010]. Results were equivalent to those found in our samples: the temperatures were much too low for $a_{TiO2} = 1$ (as little as 205°C and therefore well below the BPT), while temperatures corresponding to the original results, which are in accordance to the metamorphic record of the rocks, were obtained for $a_{TiO2} = 0.2–0.3$.

[29] There is no simple geological explanation as to why the Ti-in-quartz content would equilibrate at significantly lower temperatures (by up to ~150°C) than suggested by the synkinematic metamorphic assemblages and the thermal structure of the contact aureole. It is also not clear why the a_{TiO2} in quartz mylonites would be so low (0.2–0.3) in contrast to a_{TiO2} of 1, or close to 1, as generally proposed for metapelites [e.g., *Ghent and Stout*, 1984]. The a_{TiO2} can be calculated using ideal exchange equilibria between coexisting FeTi oxides [*Reid et al.*, 2010; *Wark et al.*, 2007]. Ideally, P and T could be determined simultaneously by the crossing isopleths method [*Thomas et al.*, 2010], combining Ti-in-quartz [*Thomas et al.*, 2010] with Zr-in-rutile [*Tomkins et al.*, 2007] or Zr-in-titanite [*Hayden and Watson*, 2007]. However, neither method can be applied in monomineralic quartz mylonites, because they are usually poor in FeTi oxides. Even if the latter were present in the quartz mylonites they were most likely not in equilibrium with the dynamically recrystallizing quartz; most of these assemblages may have formed prior to dynamic recrystallization. Hence, it may be hypothesized that dynamic recrystallization either strongly in-

fluences the a_{TiO2} or results in an apparent value of a_{TiO2}. Therefore, the traditional way to calculate a_{TiO2} based on volume diffusion, assuming static conditions and assemblages in equilibrium [e.g., *Ghent and Stout*, 1984], may not apply for mylonites. Metamorphic (re)crystallization is driven by the energy associated with the overstepping of reactions. The diffusion of components toward and away from the migrating reaction front or phase boundary usually limits the migration rate itself [*Carlson*, 2002]. On the contrary, dynamic recrystallization of minerals is mainly driven by internal strain energy and stress gradients and involves processes that operate at different time scales than the metamorphic reaction. Hence, there are clear differences between the static and the dynamic case, and some aspects of "dynamic diffusion" will be discussed in section 5.4.

[30] Based on the results and the recalculated published data [*Kohn and Northrup*, 2009], it may be suggested that $a_{TiO2} \approx 0.2–0.3$ is a more realistic value for quartz mylonites with low contents in FeTi oxides. It is, however, unlikely that the a_{TiO2} was constant across the SMZ. Because the samples from zones of SGR and BLG yielded inherited temperatures attained by slow, long cooling from pre-Alpine metamorphism, their Ti-in-quartz concentration could have been adjusted to decreasing temperature and pressure by volume diffusion and at an a_{TiO2} closer to 1, as expected for pelitic rocks [*Ghent and Stout*, 1984]. The minimum temperatures of these samples at $a_{TiO2} = 1$ of ~250–310°C (Figure 5 and Table 1) are therefore the more likely TitaniQ results, which are also consistent with the estimated ambient temperature of ~250°C before the onset of Oligocene magmatism and SMZ shearing [*Stipp et al.*, 2004]. Systematic experimental investigations and measurements on naturally deformed rocks are required to constrain a_{TiO2} and to investigate other parameters that are potentially critical for an application and extrapolation of the experimental TitaniQ calibration to natural quartz mylonites.

5.3. Temperature Heterogeneities

[31] The measured sample temperatures are in accordance with the complex thermal history caused by the cooling contact aureole during ongoing deformation and, in general, also with variable deformation microstructures consisting of old porphyroclasts and new recrystallized grains. The samples from zones of BLG and SGR deformed at temperatures < ~540°C (TN2–6, TN17 and 15.2) show only unimodal Gaussian within-sample Ti distributions and very homogeneous, flat CL. The estimated temperatures scatter between ~320 and ~390°C (at $a_{TiO2} = 0.2$, or rather, at $a_{TiO2} = 1$ between ~250 and ~310°C, see section 5.2) and there is a lack of correlation of temperatures to the peak synkinematic temperature or to the distance from the pluton (Figure 5). The related trace element data may represent the pre-Alpine amphibolite and retrograde greenschist facies metamorphic conditions of the Edolo schists [*Spalla et al.*, 1999]. Oligocene contact metamorphism and subsequent shearing and retrogression are only of very little importance as indicated by the lack of CL zoning and small within-sample scatter in trace element compositions (Figure 5 and Table 1). We propose, therefore, that the Ti-in-quartz concentration in the BLG and SGR samples is close to the "starting composition" from which the hotter GBM samples were reequilibrated. The scatter in temperatures between the samples may reflect the great sensitivity of the TitaniQ to slight variations of the Ti-in-quartz content at low temperatures (see e.g., Figure 5b). Preservation of pre-Tonale trace element concentration in quartz can be explained by the short duration of contact metamorphism, slow diffusion rates at low temperatures, the large quartz grain size of the protolith, and incomplete dynamic recrystallization during deformation (see sections 5.3 to 5.5).

[32] Samples from the GBM zone also show unimodal Gaussian temperature distributions and flat CL, which, along with the decreasing temperature trend, can be related to the Oligocene contact metamorphism and deformation. One exception is sample TN11 with its distinct CL pattern in which a temperature difference of ~75°C between the brighter grain cores and darker rims was observed (~510°C and ~435°C, respectively). Although sample TN11 is from the GBM zone (Figure 1), it is characterized by an SGR microstructure consisting of large porphyroclasts with internal subgrains and surrounded by small recrystallized grains (Figure 2f). The porphyroclasts, characterized by some GBM microstructures, were formed close to the peak synkinematic temperature (~550°C), while the recrystallized matrix corresponds to retrograde overprinting by SGR. The porphyroclast cores are within the apparent T gradient of the samples (TN12–15, 68.2 and 18.5), while the rims deviate toward lower temperatures. Hence, sample TN11 represents an exception, as retrograde overprinting by SGR is related to a resetting of Ti-in-quartz concentrations. In contrast to the SGR and BLG zone samples, this sample from the GBM

zone acquired the SGR microstructure during retrograde deformation along the SMZ. This implies that reequilibration from a higher to a lower Ti content is easier and faster than the diffusion required for an increase in Ti concentration, which is apparently in disagreement with diffusion laws. This discrepancy could be explained by an equilibration time that is longer at retrograde SGR conditions (at and below ~540°C) than at peak synkinematic temperature within the zone of SGR. Alternatively, it can be assumed that the reequilibration from higher to lower Ti content is preferred, because excess Ti can be exsolved as tiny rutile needles or TiO_2 in the colloidal state [*Cherniak and Watson*, 2007], while an increase in Ti content during temperature rise requires a Ti source in the rock, which is not necessarily given in the quartz veins. We favor this second explanation or a combination of both.

[33] Samples 110.8 and 66.3, taken closest to the intrusion (Figure 5), show *c* axis pole figures with secondary maxima close to *X* [*Stipp et al.*, 2002b], indicative of high temperature deformation above ~630–650°C [cf. *Blumenfeld et al.*, 1986; *Kruhl*, 1996; *Mainprice et al.*, 1986] as expected at the position of these samples in the contact aureole. Their GBM microstructures without any indication of microstructural overprinting display the largest recrystallized grain sizes of the entire sample set. As there is a consistent trend of increasing recrystallized grain size and hence decreasing flow stress with increasing temperature in the entire section across the SMZ [*Stipp et al.*, 2002b], it is reasonable to assume the highest deformation temperature for these two samples. Although a retrograde reequilibration of the two samples is not evident, they show significantly lower TitaniQ temperatures than expected from the peak synkinematic temperature trend (see Figure 5). One possible explanation is a partial reequilibration due to static volume diffusion without dynamic recrystallization when deformation ceased at still high contact metamorphic temperatures. Alternatively, there might be a yet unrecognized effect of the β to α quartz transition during cooling through ~645°C (at 275 MPa [*Shen et al.*, 1993]) causing some Ti release from the lattice, although no difference in Ti solubility between the two polymorphs [*Thomas et al.*, 2010] and also no difference in the recrystallization microstructure and its stress dependence [*Stipp et al.*, 2006] have experimentally been observed.

[34] There is a larger within-sample spread of *T* in the GBM mylonites than in the BLG and SGR mylonites (Figure 5 and Table 1), which could be caused by the time dependence of resetting. The resetting time was short and the reequilibration patchy in the GBM samples while the BLG and SGR samples were not reequilibrated in Ti and other trace element composition during the Oligocene contact metamorphism. The better; i.e., longer, equilibrated samples preserving the long-lasting pre-Alpine regional metamorphism of the Edolo schists also show a small *T* scatter between the measurement spots.

5.4. Diffusion Rates

[35] The distances of diffusional alteration of Ti concentrations in quartz in 1 Ma are approximately 340 μm at 800°C, 10 μm at 600°C, 1 μm at 500°C, and ~0.2 μm at 400°C [*Cherniak et al.*, 2007]. These very slow diffusion rates greatly limit the applicability of TitaniQ to gauge the deformation temperature, because the duration of plastic shearing along a ductile shear zone is usually on the order of 10^6 a, which is at $T < 600$°C not sufficient to homogeneously reset the Ti concentration in quartz grains >10 μm. Dynamic recrystallization preferentially reduces the grain size in mylonitic shear zones, whereas a smaller recrystallized grain size indicative of higher flow stress is commonly related to lower *T* of deformation [e.g., *Stipp et al.*, 2002a, 2010]. With decreasing grain size the diffusional distance for trace elements decreases, but, with decreasing *T*, the Ti diffusivity decreases even faster [*Cherniak et al.*, 2007]; eventually, at a threshold *T*, Ti diffusion virtually stops even in the case of continuous deformation over long geological time scales. Therefore, in low temperature mylonites, TitaniQ preferentially records inherited temperatures. In the investigated mylonites with a high content of porphyroclasts, temperatures below ~500°C can thus be considered to be related to the pre-Alpine metamorphism of the region, which lasted significantly longer than the thermal pulse of Adamello contact metamorphism. In contrast, in the zone of GBM, where the grains have a size of 0.2–5 mm, even a relatively short period of deformation at peak synkinematic temperatures (540–700°C) was observed to be sufficient to reequilibrate the Ti-in-quartz concentration. However, according to the experimental results [cf. *Cherniak and Watson*, 2007], a $T < 700$°C during 1 Ma is not sufficient to homogeneously reequilibrate the Ti concentration by volume diffusion in such large grains. It is, therefore, proposed that recrystallization by GBM (see section 5.5) along with diffusion via grain boundary fluids charged with trace elements [e.g., *Knipe and McCaig*, 1994]

enabled the equilibration of the Ti-in-quartz concentrations.

[36] The correlation of Al concentration to the distance from the pluton contact in the GBM zone (Figure 4) suggests that the Al content has reequilibrated in this zone in a similar fashion as the Ti-in-quartz concentration. Information on intergranular diffusivity of Al during metamorphic reactions [*Carlson*, 2002, Figure 17] can be used to estimate the time needed to redistribute Al across the given distance (0.2–5 mm) at related T (540–700°C). Similar to Ti, the calculations indicate that the Al content in the largest quartz grains could have been redistributed only at the maximum registered temperature if the deformation lasted at least 1 Ma. Since Al has been redistributed even at the lowest T in the GBM zone during much less than 1 Ma, this suggests that dynamic recrystallization by GBM may have caused the redistribution of Al and, thus, other trace elements as well.

5.5. Dynamic Recrystallization

[37] It can be suggested that trace element concentrations more than 300 m away from the pluton preserve the state prior to contact metamorphism and Tonale shearing, because they do not show a correlation to a decreasing temperature with increasing distance from the pluton, but rather fairly constant values. At the transition from SGR to GBM there is a sharp break in slope of Al and Ti concentration versus distance from the pluton (Figure 4). The break in the slope of Fe concentration is at higher temperature, possibly implying a lower temperature dependence (Figure 4). The Li concentration clearly steps up at the SGR/GBM transition, but there is no systematic increase with increasing temperature, which is probably due to the role of Li as a charge compensator. Therefore, we propose that Al, and especially Ti, are good indicators for diffusion and recrystallization effects. Indeed, both trace elements show a consistent trend of increasing concentration with decreasing distance from the pluton within the internal 300 m of the contact aureole (>540°C) except for a slight spread in the data and the deviation of the two samples closest to the contact (Figure 4; see also section 5.3). As has been discussed before, the new equilibration could not have been caused by volume diffusion, because diffusion rates are too slow to reequilibrate the samples in the given time spans (see section 5.4). The only plausible explanation is that Ti and Al contents have been modified by migration of the grain boundaries during dynamic recrystallization by GBM. Thus, in the GBM zone, within which all the samples have been completely recrystallized near peak synkinematic temperatures [cf. *Stipp et al.*, 2002b], Ti and Al concentrations in quartz were fully reset.

[38] In the zones of BLG and SGR, quartz was dynamically recrystallized to a progressively larger volume percentage and size of the new grains with increasing temperature [*Stipp et al.*, 2002b]. In the samples from the BLG zone it was difficult to measure the trace element content of the recrystallized grains owing to their small size (~5–25 μm, which is lesser than the analytical spot) and volume percentage (<10%). The data from the only measured sample are consistent with the data from the SGR samples (Figures 4 and 5). The SGR samples have ~15–80 volume percentage of recrystallized grains, and the recrystallized grain size is larger (~40–100 μm). Within the SGR samples it was possible to measure the two different grain populations (porphyroclasts and recrystallized grains) as demonstrated by the SGR-retrogressed sample TN11 from the zone of GBM (see section 5.3). Nevertheless, it can be confidently stated that the recrystallized grains do not show a trace element content different from that of the porphyroclasts as suggested by the absence of CL patterns and the small within-sample variations in Ti and other trace element content. The best explanation is that the thermal exposure time during SMZ activity was not long enough at $T < 540$°C for the reequilibration by volume diffusion, and that the dynamic recrystallization by BLG or SGR, did not mobilize the trace elements in quartz.

[39] Recrystallization is known to be an effective mechanism for isotopic resetting in shear zones [*Stünitz*, 1998]. The enhanced compositional exchange rate during deformation may result from a reduction in grain size (shorter distance for volume diffusion and larger contribution of grain boundary diffusion), or the migration of high angle grain boundaries through strained grains during recrystallization in the dislocation creep regime [*Yund and Tullis*, 1991]. It is commonly assumed that the migration of high-angle grain boundaries through the material provides high diffusivity pathways for the rapid exchange of components during recrystallization. Compositional change may thus be promoted by dislocations sweeping through a region of a mineral undergoing plastic deformation where these dislocations provide mobile shortcuts [*Chakraborty*, 2008].

[40] Experiments on polycrystalline calcite [*McCaig et al.*, 2007] have demonstrated that grain boundary diffusion of ^{44}Ca is at least five orders of magnitude greater in mobile grain boundaries than in static boundaries under the same conditions. The most likely explanation is that diffusivity in the boundaries is enhanced during migration. It has also been established that dislocations can transport atoms through a crystal by pipe diffusion at rates orders of magnitude faster than by volume diffusion [*Legros et al.*, 2008]. Because the dislocation density in deforming minerals is high, pipe diffusion probably plays an important role in mass transfer. Although data from this study do not provide direct information on grain boundary or dislocation scales, they do show that dynamic recrystallization by GBM fundamentally enhances the resetting of Ti and other trace element concentrations in quartz. Based on the existing experimental results, we conclude that the increased diffusivity along mobile grain boundaries is the most important process of reequilibration in the investigated quartz mylonites. If pipe diffusion is also significant, it has to be much more efficient at higher temperature GBM than at temperatures of SGR and BLG.

6. Summary and Conclusions

[41] The Ti-in-quartz geothermometer (TitaniQ) was applied to quartz mylonites with well-constrained metamorphic temperatures ranging between ~330 and ~690°C, as derived from reaction isograds of synkinematic mineral assemblages, with the aim to determine the deformation temperature of quartz mylonites. We found that the application of TitaniQ to quartz mylonites is not so straightforward as previously proposed. Ti solubility in quartz is highly pressure-dependent and the TiO_2 activity (a_{TiO2}) is difficult to determine precisely. When using the pressure-dependent calibration by *Thomas et al.* [2010] with an a_{TiO2} close to 1 as commonly assumed for metapelitic rocks, the resulting temperatures are much too low, suggesting that either standard a_{TiO2} estimations are wrong or the TitaniQ cannot be simply extrapolated and applied to naturally deformed rocks. This discrepancy requires further experimental investigation and systematic application of TitaniQ to different quartz mylonites before it can be used as a standard tool to determine P/T conditions of natural shear and fault zones.

[42] Assuming that TitaniQ can be applied directly to the investigated quartz mylonites, we determined the a_{TiO2} by inserting the synkinematic metamorphic P/T data from the sample with the highest Ti concentration into the temperature equation. The resulting synkinematic a_{TiO2} of 0.2 was then used to calculate the maximum TitaniQ temperatures of all other samples: the minimum temperature is constrained by $a_{TiO2} = 0.3$. We are aware that this procedure is a circular reasoning and that the calculated temperatures, although more precise, cannot be more accurate than the temperatures derived from the synkinematic mineral assemblages. However, as most of the investigated samples are mylonitic quartz veins within a relatively homogeneous sequence of metapelitic to metapsammitic rocks for which the assumption of a more or less constant a_{TiO2} is reasonable, and as the results of the trace element analysis are consistent, we are confident that this procedure is acceptable.

[43] With regard to the trace element composition of quartz there are samples which are unaffected by contact metamorphism and Tonale shearing and those which show a resetting in trace element concentration. Ti and Al data in particular, show a sharp transition from samples with a decreasing concentration with decreasing peak synkinematic temperature to samples with a fairly constant concentration caused by pre-Alpine regional metamorphism. This shift corresponds exactly to the GBM to SGR transition at 540°C. For all GBM samples, it was observed that TitaniQ registers the temperature at which quartz "locks in" its microstructure; i.e., when deformation and dynamic recrystallization ceases. Based on new SHRIMP zircon U/Pb dating of the Presanella tonalite (30.5 ± 0.5 Ma), we further ascertain that the time of contact metamorphism was very short, on the order of 1 Ma. The time of deformation at the particular peak synkinematic metamorphic conditions was actually much shorter than that. Therefore, the available time was insufficient to reequilibrate the trace element composition of quartz by volume diffusion. The best explanation for the reequilibration in the zone of GBM is an increased diffusivity along the migrating grain boundaries of the investigated quartz mylonites.

[44] Hence, dynamic recrystallization by fast grain boundary migration in the zone of GBM was a very effective reequilibration mechanism for Ti and other trace elements, while within the zones of BLG and SGR no reequilibration of the Ti concentrations could be detected. Grain boundary migration recrystallization is likely one of the most important processes for the enhancement of diffusive equilibration during deformation and it is

much faster than equilibration under static conditions by volume and grain boundary diffusion.

Acknowledgments

[45] Acknowledgment is given to the motivating discussions with F. Mazdab and J. Vazquez, with grateful thanks to D. Campbell, I. Coutand, and U. Martens for their help with the SHRIMP measurements and to Joel Baker for editorial work. Critical comments on an earlier version of the manuscript by M. Bestmann, E. Mariani, and J. Thomas and the thorough reviews by D. Prior and G. Pennacchioni greatly helped to improve our work. Jay Thomas in the Department of Earth and Environmental Sciences at Rensselaer Polytechnic Institute kindly provided the reference sample QTiP 13. The study was supported by the Natural Sciences and Engineering Research Council of Canada (NSERC), Blaustein Foundation (Stanford University), and the National Science Foundation (USA).

References

Blumenfeld, B., D. Mainprice, and J. L. Bouchez (1986), C-slip in quartz in subsolidus deformed granites, *Tectonophysics*, *127*, 97–115, doi:10.1016/0040-1951(86)90081-8.

Carlson, W. (2002), Scales of disequilibrium and rates of equilibration during metamorphism, *Am. Mineral.*, *87*, 185–204.

Chakraborty, S. (2008), Diffusion in solid silicates: A tool to track timescales of processes comes of age, *Annu. Rev. Earth Planet. Sci.*, *36*, 153–190, doi:10.1146/annurev.earth.1136.031207.124125.

Cherniak, D. J., and E. B. Watson (2007), Ti diffusion in zircon, *Chem. Geol.*, *242*(3–4), 473–486.

Cherniak, D. J., E. B. Watson, and D. A. Wark (2007), Ti diffusion in quartz, *Chem. Geol.*, *236*, 65–74, doi:10.1016/j.chemgeo.2006.09.001.

Del Moro, A. G., G. Pardini, C. Quercioli, I. M. Villa, and E. Callegari (1983), Rb/Sr and K/Ar chronology of Adamello granitoids, southern Alps, *Mem. Soc. Geol. Ital.*, *26*, 285–299.

Dennen, W. H., W. H. Blackburn, and A. Quesada (1970), Aluminum in quartz as a geothermometer, *Contrib. Mineral. Petrol.*, *27*, 332–342, doi:10.1007/BF00389817.

Ferry, J. M., and E. B. Watson (2007), New thermodynamic models and revised calibrations for the Ti-in-zircon and Zr-in-rutile thermometers, *Contrib. Mineral. Petrol.*, *154*(4), 429–437, doi:10.1007/s00410-007-0201-0.

Gansser, A., and N. Pantic (1988), Prealpine events along the eastern Insubric Line (Tonale Line, northern Italy), *Eclogae Geol. Helv.*, *81*, 567–577.

Ghent, E., and M. Stout (1984), TiO_2 activity in metamorphosed pelitic and basic rocks: Principles and applications to metamorphism in southeastern Canadian Cordillera, *Contrib. Mineral. Petrol.*, *86*(3), 248–255, doi:10.1007/BF00373670.

Götze, J., M. Plötze, M. Tichomirowa, H. Fuchs, and J. Pilot (2001), Aluminium in quartz as an indicator of the temperature of formation of agate, *Mineral. Mag.*, *65*(3), 407–413, doi:10.1180/002646101300119484.

Grujic, D., M. Stipp, and J. L. Wooden (2009), Thermometry of quartz mylonites, *Geochim. Cosmochim. Acta*, *73*(13), suppl. 1, A472–A472, doi:10.1016/j.gca.2009.05.025.

Hansmann, W., and F. Oberli (1991), Zircon inheritance in an igneous rock suite from the southern Adamello batholith (Italian Alps). Implications for petrogenesis, *Contrib. Mineral. Petrol.*, *107*, 501–518, doi:10.1007/BF00310684.

Hayden, L. A., and E. B. Watson (2007), Rutile saturation in hydrous siliceous melts and its bearing on Ti-thermometry of quartz and zircon, *Earth Planet. Sci. Lett.*, *258*(3–4), 561–568, doi:10.1016/j.epsl.2007.04.020.

Heitzmann, P. (1987), Evidence of late Oligocene/Early Miocene backthrusting in the central Alpine "root zone," *Geodin. Acta*, *1*(3), 183–192.

Jessell, M. W. (1987), Grain-boundary migration microstructures in a naturally deformed quartzite, *J. Struct. Geol.*, *9*, 1007–1014, doi:10.1016/0191-8141(87)90008-3.

Kawasaki, T., and Y. Osanai (2008), Empirical thermometer of TiO_2 in quartz for ultrahigh-temperature granulites of East Antarctica, in *Geodynamic Evolution of East Antarctica*, edited by M. Satish-Kumar et al., *Geol. Soc. Spec. Publ.*, *308*, 419–430, doi:10.1144/SP1308.1121.

Kirschner, D. L., Z. D. Sharp, and H. Masson (1995), Oxygen isotope thermometry of quartz-calcite veins: Unraveling the thermal-tectonic history of the subgreenschist facies Morcles nappe (Swiss Alps), *Geol. Soc. Am. Bull.*, *107*(10), 1145–1156, doi:10.1130/0016-7606(1995)107<1145:OITOQC>2.3.CO;2.

Knipe, R., and A. M. McCaig (1994), Microstructural and microchemical consequences of fluid flow in deforming rocks, in *Geofluids: Origin, Migration and Evolution of Fluids in Sedimentary Basins*, edited by J. Parnell, *Geol. Soc. Spec. Publ.*, *78*, 99–111.

Kohlstedt, D. L., B. Evans, and S. J. Mackwell (1995), Strength of the lithosphere: Constraints imposed by laboratory experiments, *J. Geophys. Res.*, *100*, 17,587–17,602.

Kohn, M. J., and C. J. Northrup (2009), Taking mylonite's temperatures, *Geology*, *37*(1), 47–50, doi:10.1130/G25081A.1.

Kruhl, J. H. (1996), Prism- and basal-plane parallel subgrain boundaries in quartz; a microstructural geothermobarometer, *J. Metamorph. Geol.*, *14*(5), 581–589, doi:10.1046/j.1525-1314.1996.00413.x.

Larsen, R. B., I. Henderson, P. M. Ihlen, and F. Jacamon (2004), Distribution and petrographic behaviour of trace elements in granitic pegmatite quartz from southern Norway, *Contrib. Mineral. Petrol.*, *147*, 615–628, doi:10.1007/s00410-00004-00580-00414.

Legros, M., G. Dehm, E. Arzt, and T. J. Balk (2008), Observation of giant diffusivity along dislocation cores, *Science*, *319*, 1646–1649, doi:10.1126/science.1151771.

Ludwig, K. R. (2003), Isoplot 3.0: A geochronological toolkit for Microsoft Excel, *Spec. Publ. 4*, 70 pp., Berkeley Geochronol. Cent., Berkeley, Calif.

Ludwig, K. R., and R. Mundil (2002), Extracting reliable U-Pb ages and errors from complex populations of zircons from Phanerozoic tuffs, *Geochim. Cosmochim. Acta, 66*, A463.

Macdonald, R., R. L. Smith, and J. E. Thomas (1992), *Chemistry of the Subalkalic Silicic Obsidians*, *U.S. Geol. Surv. Prof. Pap.*, *1523*, 214 pp.

Mainprice, D., J.-L. Bouchez, P. Blumenfeld, and J. M. Tubià (1986), Dominant c slip in naturally deformed quartz: Implications for dramatic plastic softening at high temperature, *Geology*, *14*, 819–822, doi:10.1130/0091-7613(1986)14<819:DCSIND>2.0.CO;2.

Maschmeyer, D., and G. Lehmann (1983), New hole centers in natural quartz, *Phys. Chem. Miner.*, *10*, 84–88, doi:10.1007/BF00309589.

Mayer, A., G. Cortiana, G. V. Dal Piaz, E. Deloule, R. De Pieri, and P. Jobstraibizer (2003), U–Pb single zircon ages of the Adamello batholith, Southern Alps, *Mem. Sci. Geol.*, *55*, 151–167.

McCaig, A., S. Covey-Crump, W. Ben Ismaïl, and G. Lloyd (2007), Fast diffusion along mobile grain boundaries in calcite, *Contrib. Mineral. Petrol.*, *153*(2), 159–175, doi:10.1007/s00410-006-0138-8.

Mulch, A., C. Teyssier, M. A. Cosca, and C. P. Chamberlain (2007), Stable isotope paleoaltimetry of Eocene core complexes in the North American Cordillera, *Tectonics*, *26*, TC4001, doi:10.1029/2006TC001995.

Pennacchioni, G., G. Di Toro, P. Brack, L. Menegon, and I. M. Villa (2006), Brittle-ductile-brittle deformation during cooling of tonalite (Adamello, Southern Italian Alps), *Tectonophysics*, *427*(1–4), 171–197, doi:10.1016/j.tecto.2006.05.019.

Pennacchioni, G., L. Menegon, B. Leiss, F. Nestola, and G. Bromiley (2010), Development of crystallographic preferred orientation and microstructure during plastic deformation of natural coarse-grained quartz veins, *J. Geophys. Res.*, *115*, B12405, doi:10.1029/2010JB007674.

Pomella, H., U. Klötzli, R. Scholger, M. Stipp, and B. Fügenschuh (2011), The Northern Giudicarie and the Meran-Mauls fault (Alps, northern Italy) in the light of new paleomagnetic and geochronological data from boudinaged Eo-/Oligocene tonalites, *Int. J. Earth Sci.*, doi:10.1007/s00531-010-0612-4, in press.

Press, W. H., B. P. Flannery, S. A. Teukolsky, and W. T. Vetterling (1992), *Numerical Recipes in FORTRAN: The Art of Scientific Computing*, 2nd ed., 697 pp., Cambridge Univ. Press, Cambridge, U. K.

Rakov, L. T. (2006), Mechanisms of isomorphic substitution in quartz, *Geochem. Int.*, *44*(10), 1004–1014, doi:10.1134/S0016702906100053.

Reid, M. R., J. A. Vazquez, and A. K. Schmitt (2010), Zircon-scale insights into the history of a supervolcano, Bishop Tuff, Long Valley, California, with implications for the Ti-in-zircon geothermometer, *Contrib. Mineral. Petrol.*, *161*, 1–19, doi:10.1007/s00410-00010-00532-00410.

Sato, K., and M. Santhosh (2007), Titanium-in-quartz as a record of ultrahigh-temperature metamorphism: The granulites of Karur, southern India, *Mineral. Mag.*, *71*(2), 143–154, doi:10.1180/minmag.2007.071.2.143.

Schmid, S. M., H. R. Aebli, F. Heller, and A. Zingg (1989), The role of the Periadriatic Line in the tectonic evolution of the Alps, in *Alpine Tectonics*, edited by M. P. Coward, D. Dietrich, and R. G. Park, *Geol. Soc. Spec. Publ.*, *45*, 153–171.

Shen, A. H., W. A. Bassett, and I. M. Chou (1993), The α–β quartz transition at high-temperatures and pressures in a diamond-anvil cell by laser interferometry, *Am. Mineral.*, *78*(7–8), 694–698.

Spalla, M. I., E. Carminati, S. Ceriani, A. Olivia, and D. Battaglia (1999), Influence of deformation partitioning and metamorphic re-equilibration on P-T path reconstruction in the pre-Alpine basement of central Southern Alps, *J. Metamorph. Geol.*, *17*, 319–336, doi:10.1046/j.1525-1314.1999.00199.x.

Stipp, M., H. Stünitz, R. Heilbronner, and S. M. Schmid (2002a), Dynamic recrystallization of quartz: Correlation between natural and experimental conditions, in *Deformation Mechanisms, Rheology and Tectonics; Current Status and Future Perspectives*, edited by S. de Meer et al., *Geol. Soc. Spec. Publ.*, *200*, 171–190.

Stipp, M., H. Stünitz, R. Heilbronner, and S. M. Schmid (2002b), The eastern Tonale fault zone: A 'natural laboratory' for crystal plastic deformation of quartz over a temperature range from 250 to 700°C, *J. Struct. Geol.*, *24*, 1861–1884, doi:10.1016/S0191-8141(02)00035-4.

Stipp, M., B. Fügenschuh, L. P. Gromet, H. Stünitz, and S. M. Schmid (2004), Contemporaneous plutonism and strike-slip faulting: A case study from the Tonale fault zone north of the Adamello pluton (Italian Alps), *Tectonics*, *23*, TC3004, doi:10.1029/2003TC001515.

Stipp, M., J. Tullis, and H. Behrens (2006), Effect of water on the dislocation creep microstructure and flow stress of quartz and implications for the recrystallized grain size piezometer, *J. Geophys. Res.*, *111*, B04201, doi:10.1029/2005JB003852.

Stipp, M., J. Tullis, M. Scherwath, and J. H. Behrmann (2010), Dynamically recrystallized grain size distributions indicate mechanism changes, *Geology*, *38*, 759–762, doi:10.1130/G31162.31161.

Stöckhert, B., M. R. Brix, R. Kleinschrodt, A. J. Hurford, and R. Wirth (1999), Thermochronometry and microstructure of quartz—A comparison with experimental flow laws and predictions on the temperature of the brittle-plastic transition, *J. Struct. Geol.*, *21*, 351–369, doi:10.1016/S0191-8141(98)00114-X.

Stünitz, H. (1998), Syndeformational recrystallization—Dynamic or compositionally induced?, *Contrib. Mineral. Petrol.*, *131*(2–3), 219–236, doi:10.1007/s004100050390.

Thomas, J. B., E. B. Watson, F. S. Spear, P. T. Shemella, S. K. Nayak, and A. Lanzirotti (2010), TitaniQ under pressure: The effect of pressure and temperature on the solubility of Ti in quartz, *Contrib. Mineral. Petrol.*, *160*, 743–759, doi:10.1007/s00410-010-0505-3.

Tomkins, H. S., R. Powell, and D. J. Ellis (2007), The pressure dependence of the zirconium-in-rutile thermometer, *J. Metamorph. Geol.*, *25*, 703–713, doi:10.1111/j.1525-1314.2007.00724.x.

Tullis, J. (2002), Deformation of granitic rocks: Experimental studies and natural examples, *Rev. Mineral. Geochem.*, *51*(1), 51–95, doi:10.2138/gsrmg.51.1.51.

Urai, J. L., W. D. Means, and G. S. Lister (1986), Dynamic recrystallization of minerals, in *Mineral and Rock Deformation: Laboratory Studies—The Paterson Volume*, *Geophys. Monogr. Ser.*, vol. 36, edited by B. E. Hobbs and H. C. Heard, pp. 161–199, AGU, Washington, D. C.

Valcke, S. L. A. (2008), EBSD analysis of heterogeneous microstructures in experimentally deformed calcite: Development of core and mantle subgrains, grain boundary bulges and recrystallised grains, Ph.D. thesis, 143 pp., Utrecht Univ., Utrecht, Netherlands.

van Daalen, M., R. Heilbronner, and K. Kunze (1999), Orientation analysis of localized shear deformation in quartz fibres at the brittle-ductile transition, *Tectonophysics*, *303*, 83–107, doi:10.1016/S0040-1951(98)00264-9.

Vannay, J.-C., Z. D. Sharp, and B. Grasemann (1999), Himalayan inverted metamorphism constrained by oxygen isotope thermometry, *Contrib. Mineral. Petrol.*, *137*, 90–101, doi:10.1007/s004100050584.

Voll, G. (1976), Recrystallization of quartz, biotite and feldspars from Erstfeld to the Leventina Nappe, Swiss Alps, and its geological significance, *Schweiz. Mineral. Petrogr. Mitt.*, *56*, 641–647.

Wark, D. A., and E. B. Watson (2006), TitaniQ: A titanium-in-quartz geothermometer, *Contrib. Mineral. Petrol.*, *152*, 743–754, doi:10.1007/s00410-006-0132-1.

Wark, D. A., W. Hildreth, F. S. Spear, D. J. Cherniak, and B. E. Watson (2007), Pre-eruption recharge of the Bishop magma system, *Geology*, *35*(3), 235–238; doi:10.1130/G23316A.23311.

Watson, E. B., D. A. Wark, and J. B. Thomas (2006), Crystallization thermometers for zircon and rutile, *Contrib. Mineral. Petrol.*, *151*, 413–433, doi:10.1007/s00410-006-0068-5.

Werling, E. (1992), *Tonale-, Pejo- und Judicarien-Linie: Kinematik, Mikrostrukturen und Metamorphose von Tektoniten aus räumlich interferierenden aber verschiedenaltrigen Verwerfungszonen*, 276 pp., ETH Zürich, Zurich, Switzerland.

Yund, R. A., and J. Tullis (1991), Compositional changes of minerals associated with dynamic recrystallization, *Contrib. Mineral. Petrol.*, *108*, 346–355, doi:10.1007/BF00285942.